International Journal of Pharmaceutics 419 (2011) 137–146

Contents lists available at ScienceDirect

International Journal of Pharmaceutics

journal homepage: www.elsevier.com/locate/ijpharm

Acoustic assessment of mean grain size in pharmaceutical compacts

Carson J. Smith[a,1], James D. Stephens[b], Bruno C. Hancock[c], Armin Saeedi Vahdat[b], Cetin Cetinkaya[b,*]

[a] Dept. of Chemical and Biomolecular Engineering, Clarkson University, Potsdam, NY 13699-5725, USA
[b] Dept. of Mechanical and Aeronautical Engineering, Clarkson University, Potsdam, NY 13699-5725, USA
[c] Pfizer Inc., MS 8156-006, Eastern Point Road, Groton, CT 06340, USA

ARTICLE INFO

Article history:
Received 11 May 2011
Received in revised form 8 July 2011
Accepted 21 July 2011
Available online 27 July 2011

Keywords:
Attenuation coefficient
Microstructure characteristics of compacts
Grain sizing in compacts
Ultrasonic pitch-catch method

ABSTRACT

An ultrasonic non-destructive technique for the microstructure length-scale characterization of solid dosage pharmaceutical tablets is presented. The technique is based on the relationship between the attenuation of longitudinal ultrasonic elastic waves and the size of micro-structural features in the tablet material. In the reported experiments, the ultrasonic attenuation in microcrystalline cellulose (MCC)–lactose monohydrate (LMH) blended pharmaceutical compacts is measured by means of two pitch-catch experiments. The frequency dependent attenuation coefficient for the MCC–LMH compacts is then related to the mean grain diameter for each compact. For verification purposes, the mean grain diameter of the compacts was also established using micro-scale X-ray computerized tomography (MicroXCT). The mean grain diameters established by both routines agree well, and support the efficacy of the ultrasonic attenuation technique. The microstructure of a pharmaceutical compact (i.e., grain sizes and micro-feature size distribution) has been shown to have a profound effect on its mechanical properties, namely hardness, porosity, and mass density distribution, and in turn, can critically impact the dissolution profile and structural integrity of a compact. The ultrasonic technique presented provides a non-destructive and rapid method for determining the mean grain diameter size for powder compacts, thus providing a more timely and cost-effective method, compared to traditional techniques, of characterizing a compact's internal microstructure.

1. Introduction

Presently, the most prevalent and preferred means of drug delivery is via the orally administered drug tablet. Along with capsules, tablets represent nearly 70% of all pharmaceutical preparations (Abdullah et al., 2010). While tablets are a popular vehicle for the accurate and repeatable delivery of active pharmaceutical ingredients (APIs) to the body, in order to maintain bioavailability and therapeutic effectiveness (Dokoumetzidis and Macheras, 2006), the desired dissolution profile of the tablet must be preserved throughout the manufacturing process (Azarmi et al., 2007). The dissolution profile and release rate of drug tablets are dependent upon various mechanical properties, such as hardness (Saravanan et al., 2002), and thus particle size, inter-granular bonding, and the internal microstructure of the tablet (Jounela et al., 1975; Lee, 2003; Levy, 1963; Narayan and Hancock, 2003, 2005). Thus, it is critical to drug tablet quality control that techniques for accurate and timely microstructure characterization and effective monitoring be implemented during manufacturing.

Product recalls are exorbitantly expensive and the sale of defective medicines can lead to undesirable consequences for consumers as well as their manufacturers (Oberholzer-Gee and Inamdar, 2004). To ensure tablet quality and safety, the U.S. Federal Drug Administration (FDA) released its Process Analytical Technology (PAT) initiative, encouraging the drug industry to voluntarily develop systems for "designing, analyzing, and controlling manufacturing through timely measurements (i.e., during processing) of critical quality and performance attributes of raw and in-process materials and processes, with the goal of ensuring final product quality" (Hussain et al., 2004). As a response to the PAT initiative, many manufacturers, in addition to using traditional techniques such as "hardness" and friability experiments, abrasiveness and roughness tests (Podczeck, 1998), and Scanning Electron Microscopy (SEM) (Fu et al., 2006a,b; Narayan and Hancock, 2003, 2005), have implemented various rapid and non-destructive spectroscopy-based techniques using NIR and Raman (see Roggo et al., 2007 for a review) to extract physical properties (e.g., tablet hardness, coat thickness, and particle size) from pharmaceutical tablets. However, the applicability of these techniques for mechanical testing has been reduced due to (i) their limited penetration into the tablet material, and/or (ii) their optical, and thus, indirect nature. As a result, the efficacy of rapid, inexpensive, and non-destructive ultrasonic acoustic methods for

* Corresponding author. Tel.: +1 315 268 6514; fax: +1 315 268 6695.
E-mail address: cetin@clarkson.edu (C. Cetinkaya).
[1] Current address: Specialty Materials Division, Corning Inc., Canton, NY 13617, USA.

0378-5173/$ – see front matter © 2011 Elsevier B.V. All rights reserved.
doi:10.1016/j.ijpharm.2011.07.032

microstructure and mechanical characterization is now being investigated (Varghese and Cetinkaya, 2007; Akseli et al., 2008b; Akseli and Cetinkaya, 2008a).

Ultrasonic wave attenuation is influenced by the microstructure of the medium material and thus related to various geometric and elastic parameters such as mass density distribution, grain size, dislocation density, inter-granular bonding, and porosity. This relationship between microstructure and attenuation has spurred the development of a variety of ultrasonic techniques for microstructure characterization. For example, computational and experimental ultrasonic methods have been successfully developed for the determination of particle grain size in metals and other semi-porous media. Nowacki (2009) purposed a method for sizing steel grains by measuring the attenuation of ultrasonic waves using two different ultrasonic impulse methods. Similarly, Sarpun and Kilickaya (2006) developed an ultrasonic velocity technique for the determination of marble grain size, and were successful in confirming the ultrasonic technique results via optical microscope measurements. In addition to average grain size predictions, research has also been conducted to develop mathematical procedures for relating ultrasonic attenuation to grain size distributions in polycrystalline materials (Nicoletti and Anderson, 1997).

It is documented that the size of the powder particles used to manufacture pharmaceutical compacts can influence their mechanical properties (Adolfsson et al., 1997; Alderborn and Nystrom, 1982; Sun and Grant, 2001). In most cases the use of smaller and more tightly packing particles allows a greater number of inter-granular interactions to occur, thus strengthening the compact. In addition, particle fracture and/or plastic deformation during tablet compression can lead to an increased contact area for inter-granular bonding, permitting an even larger degree of inter-granular interaction resulting in a concomitant increase in tablet strength (Hiestand, 2003). There is evidence that demonstrates that changes in the internal micro-structure of pharmaceutical tablets not only influence mechanical strength, but also impact the rate at which APIs are released from some types of dosage forms (Gane et al., 2006). For all these reasons it is highly desirable to have a greater understanding of the internal microstructure of pharmaceutical compacts (Eiliazadeh et al., 2003; Djemai and Sinka, 2006; Sinka et al., 2004). This is evidenced from the early experimental work of Lewis and Train (1965) to more modern non-destructive approaches using sophisticated analytical techniques such as microtomography (Fu et al., 2006a,b).

In recent years, ultrasonic acoustic wave methods have been developed to non-destructively characterize mechanical properties such as effective Young's modulus (Akseli et al., 2009a; Akseli and Cetinkaya, 2008a,c), effective Poisson's ratio (Akseli et al., 2008a, 2010; Akseli and Cetinkaya, 2008c), anisotropy (Akseli et al., 2009b), mean mass density (Akseli et al., 2010; Akseli and Cetinkaya, 2008c), and thickness (Akseli and Cetinkaya, 2008a,b) of pharmaceutical powder compacts. However, the potential for these and similar methods to reliably characterize compact microstructure has yet to be fully realized.

In the current study, an ultrasonic elastic wave method is applied to experimentally predict the mean grain diameter size within pharmaceutical powder compacts. Due to the fact that pharmaceutical powder compacts are composed of soft materials, individual grains often deform and conglomerate during the compaction process. As a result of the large compressive forces utilized during compaction, powder particles are progressively rearranged, forced together, and ultimately densified to a level of intense inter-granular bonding. Eventually, continued compression leads to plastic deformation and the establishment of larger microstructural features with characteristic length-scales (Narayan and Hancock, 2003, 2005). Though these larger length-scale features are attenuative and can be detected by the ultrasonic wave pulses used in the current study, the mean grain diameter in the tablet microstructure is still reliably ascertained by two methods of analyzing plots of the frequency dependent attenuation coefficient.

2. Attenuation models

Attenuation causes the relative reduction in the amplitude of a wave propagating in an attenuating material or structure. For a harmonic wave propagating in the positive x-direction, the stress or strain amplitude reduction can be expressed by:

$$A_x = A_{x_o} \exp(-\alpha(f)(x - x_o)) \tag{1}$$

where A_{x_o} is the amplitude of the stress wave travelling at frequency f (Hz) at location x_o, A_x the amplitude of the wave travelling at frequency f at location x, and α the frequency-dependent attenuation coefficient. Thus, ultrasonic attenuation is the relative amplitude reduction of an ultrasonic wave per unit length of medium, and is expressed in Np/m. If the amplitude data at two locations is available, then the attenuation coefficient can be determined by comparing the wave amplitudes at the two positions, x_o and $x = x_o + h$, as follows:

$$\alpha(f) = \frac{1}{h} \ln\left(\frac{A_{x_o}}{A_{x_o+h}}\right) \tag{2}$$

where h is the distance travelled by the harmonic wave component. The amplitude of a wave packet propagating through a pharmaceutical compact can be reduced by two dominant mechanisms: (i) wave absorption (energy dissipation due to viscoelastic effects) and/or (ii) wave scattering (reflection/redirection from boundaries and inclusions), such that:

$$\alpha(f) = \alpha_a(f) + \alpha_s(f) \tag{3}$$

where $\alpha_a(f)$ and $\alpha_s(f)$ are the frequency dependent attenuation contributed by wave absorption and wave scattering, respectively. For the purpose of mechanical characterization in metals and other structural forms, the absorption contribution to attenuation is often neglected due to its relative insignificance when compared to the scattering mechanism. This assumption yields that all attenuation is due to wave scattering:

$$\alpha(f) \approx \alpha_s(f) \tag{4}$$

where attenuation is only caused by the acoustic wave's interaction with wave scattering features such as grain boundaries, voids, inclusions, micro-cracks, macro-cracks, and other structural defects/irregularities.

Ultrasonic attenuation is also dependent upon the wavelength (frequency) of the ultrasonic pulse, grain dimensions, and other material properties of the medium through which the pulse is propagating. Concerning these dependencies, the standard modeling assumptions made for grain scattering attenuation in polycrystalline materials are: (i) grain boundary discontinuity is elastic in nature, thus allowing for a continuous density distribution; (ii) individual grains are equiaxed (e.g., spherical, cubical, or cylindrical); (iii) the crystalline structure of grains is weakly anisotropic; (iv) the number of grains is large; (v) individual grains do not scatter coherently; (vi) the scattered energy is small, allowing multiple scattering effects to be neglected.

According to Morse (1936) and Roney (1950), each grain within an attenuating material contributes to attenuation depending on the ratio of the acoustic wavelength of the propagating pulse (λ) to the mean grain diameter (D) of the material structure. Under the assumptions listed above, three classical scattering regimes have been identified and are distinguished by the acoustic wavelength to mean grain diameter ratio. In the regime corresponding to an acoustic wavelength (λ) that is much greater than the mean grain

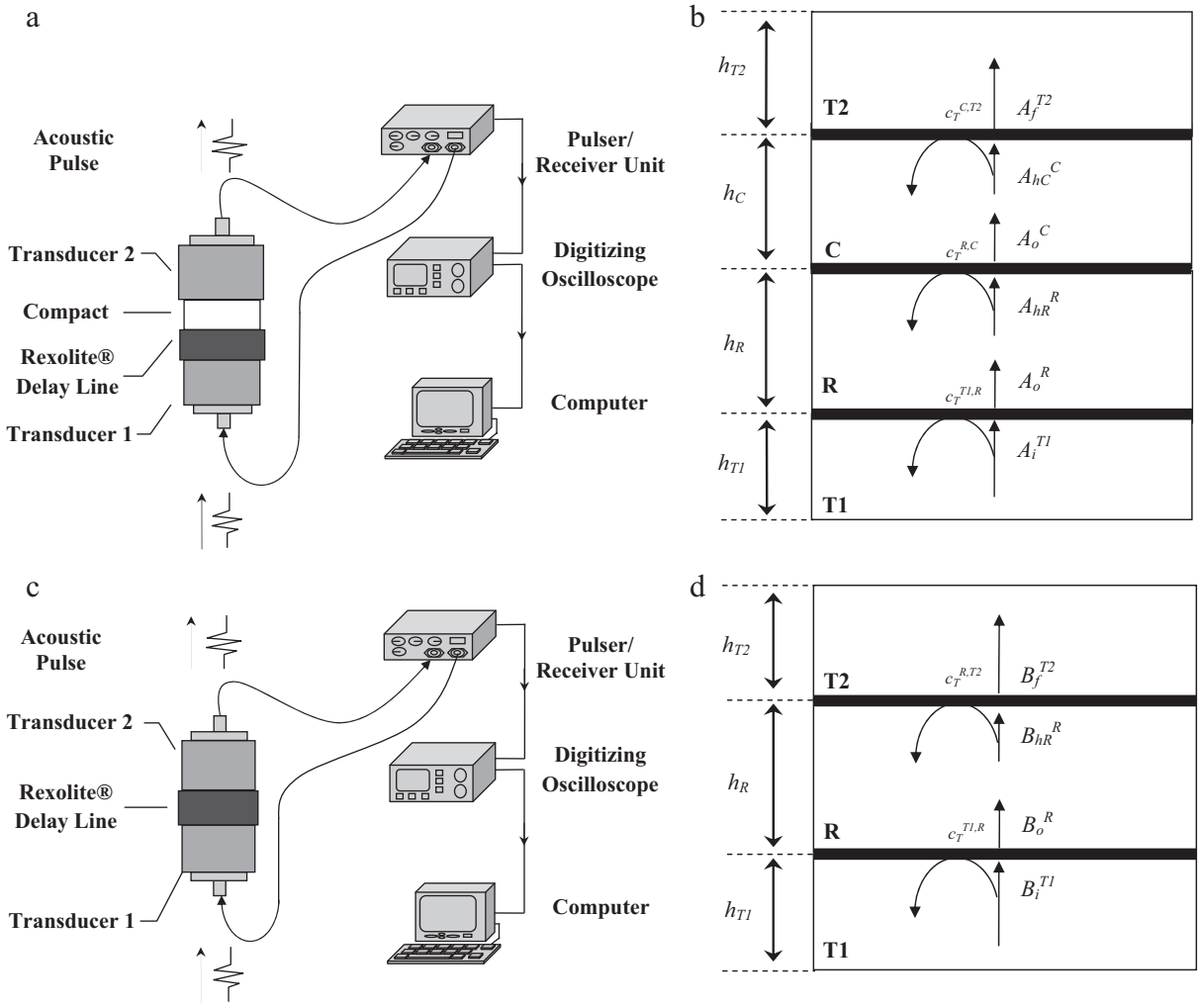

Fig. 1. (a) Instrumentation diagram of the pitch-catch experimental setup (Setup A). (b) The paths of reflection and transmission of the incident wave at the interfaces between Transducer 1 (T1), the delay line (R), the compact (C), and Transducer 2 (T2). (c) Instrumentation diagram of the pitch-catch calibration test setup (Setup B). (d) The paths of reflection and transmission of the incident wave at the interfaces between Transducer 1 (T1), the delay line (R), and Transducer 2 (T2).

diameter (D) (i.e., $\lambda \gg D$), attenuation is dominated by Rayleigh scattering, and is represented by:

$$\alpha(f, D) = C_r D^3 f^4 = \frac{C_r c_L^4 D^3}{\lambda^4} \quad (5)$$

where D is the mean grain size, f the frequency, C_r a material constant, c_L the longitudinal velocity of sound in the medium, and λ the acoustic wavelength. In the second (stochastic) regime, the acoustic wavelength is comparable to the grain diameter (i.e., $\lambda \approx D$). The attenuation in this regime is related as follows:

$$\alpha(f, D) = C_s D f^2 = \frac{C_s c_L^2 D}{\lambda^2} \quad (6)$$

where C_s is a material constant. As discussed in Botvina et al. (2000), assumption (vi) from above does not apply to the stochastic regime, where multiple scattering effects are not negligible. The third regime is characterized by an acoustic wavelength that is much smaller than the grain diameter (i.e., $\lambda \ll D$). The attenuation within this regime, called the diffusion regime, is independent of frequency and represented by the following equation:

$$\alpha(D) = \frac{C_d}{D} \quad (7)$$

where C_d is a material constant. Assumption (vi) from above is also not required for the diffusion regime since multiple scattering effects must be taken into consideration. While the three classical scattering regimes described in Eqs. (5)–(7) have been extensively applied for the analysis of ultrasonic attenuation in polycrystalline structures, the agreement between theoretical and experimental results has been considered only moderate and numerous authors have identified that materials belonging to the classical Rayleigh scattering regime, instead of demonstrating the standard f^4-attenuation dependence, often reveal frequency dependencies of other orders and the presence of non-Rayleigh scattering mechanisms (Botvina et al., 2000; Papadakis, 1965). Based on a review of the available literature concerning the correlation of ultrasonic attenuation and grain size, a general model, not constrained by the boundaries of the classical scattering regimes, for relating the ultrasonic attenuation in pure metals and alloys to grain size is proposed by Botvina et al. (2000).

The objective of the pitch-catch attenuation experimental setup described here is to measure attenuation (α) as a function of frequency (f) in tablet material, and from this data extract the mean grain diameter in the tablet microstructure. Pharmaceutical tablets can feature powder grain sizes ranging from less than 10 μm to well over 500 μm (Narayan and Hancock, 2005). Consequently, as the transducers used in the pitch-catch experimental setup

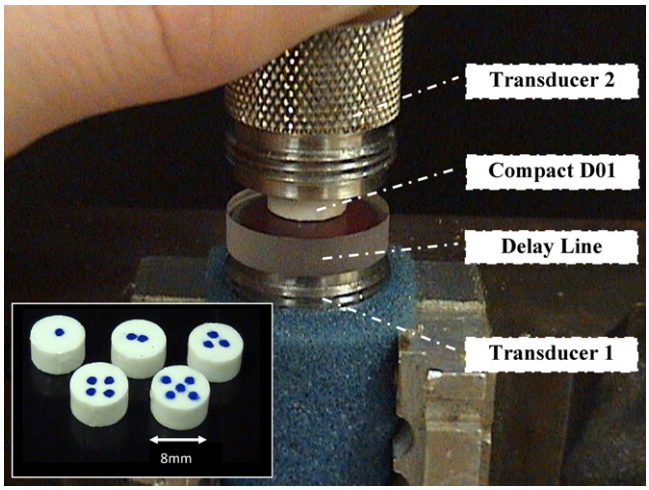

Fig. 2. Photograph of Setup A. Inset shows the five compacts utilized for the experiments.

have a frequency bandwidth of 1.10–2.80 MHz (i.e., a wavelength range of $\lambda = 1360–536\ \mu m$ for an average c_L of 1500 m/s), the scattering attenuation, according to the classical scattering regimes, ought to be dominated by the Rayleigh scattering mechanism (Eq. (5)). As most grain sizes and characteristic length scales will fall below the 536 μm threshold, the attenuation, if a result of Rayleigh scattering, ought to demonstrate a fourth power dependence on frequency. However, when plotted in the wavelength of the transducer bandwidth, the attenuation profiles for the pharmaceutical tablets tested in the current study do not demonstrate the expected fourth power dependency. Given this result, the correlation model developed by Botvina et al. (2000) was applied to the experimental attenuation profiles to reveal an experimental mean grain diameter of approximately 35.3 μm. This mean grain diameter size is consistent with the analysis of independent MicroXCT images.

3. Experimental/calibration setups

The pitch-catch attenuation experimental setup (Setup A) and pitch-catch calibration test setup (Setup B) (Fig. 1) were designed to launch and acquire ultrasonic wave pulses attenuated by pharmaceutical tablets, to determine the frequency dependent attenuation coefficient for the tested tablet material. The setups consist of an ultrasonic pulser/receiver unit (Panametrics 5077PR), one pitching transducer (Panametrics V540-SM) with a central frequency of 2.25 MHz ($\lambda = 666\ \mu m$ at $c_L = 1500$ m/s) and a −6 dB bandwidth of 1.70 MHz (1.10–2.80 MHz), one receiving transducer (Panametrics V540-SM), a Rexolite® delay line, a digitizing oscilloscope (Tektronix TDS3052), and a computer with software for data acquisition and analysis. The equipment used in these setups is similar to that used in Akseli et al. (2009a). The instrumentation and schematic diagrams of the pitch-catch attenuation experimental setup (Setup A) and the pitch-catch calibration test setup (Setup B) are depicted, respectively, in Fig. 1a–d. A photograph of the pitch-catch attenuation experimental setup (Setup A) is given in Fig. 2, with an inset of the compacts used for this investigation. In the pitch-catch attenuation experimental setup (Setup A), the pitching transducer (Transducer 1) is placed on the bottom, followed by the delay line, compact, and receiving transducer (Transducer 2). In the pitch-catch calibration test setup (Setup B), the pitching transducer (Transducer 1) is placed on the bottom, followed by the delay line, and receiving transducer (Transducer 2). The function of the delay line is to create a time lapse between the acoustic pulse generated by Transducer 1 (denoted as A_i^{T1} and as B_i^{T1} in the path tracing diagrams of Fig. 1b and d, respectively) and the arrival of any reflected waves from the transducer–compact interface. The inclusion of the delay line prevents the possible wave mixing that could result from the overlap of the acoustic pulse leaving Transducer 1 and any reflected acoustic signals. Couplant gel (UltraGel II, Sonotech Inc., Bellingham, WA) was used to ensure the transmission of the acoustic pulses through each interface. A thin enamel coating (Crystal Clear Enamel, Rust-Oleum Co., Vernon Hills, IL) was applied to each compact surface to protect the compact from being damaged by repeated use, as well as by moisture and glycerin contained in the gel. For all of the compacts tested a standard 24-h dry time was instituted before any experiments were conducted. The effects of the couplant gel and enamel coating on wave transmission are neglected due to the minimal thickness of the gel layer and enamel coat (50–100 μm) compared to the tablet thickness (3.60–4.00 mm) and measurement precision. A digital caliper (CD-6in CS Absolute Digimatic Caliper, Mitutoyo Inc., Aurora, IL) was used to measure the dimensions of the compacts and a digital scale (A120S-L, Mettler-Toledo Inc., Columbus, OH) was employed to determine the tablet mass.

4. Materials and sample tablet set

Compacts were manufactured from a placebo blend of excipients containing microcrystalline cellulose (64%, w/w), lactose monohydrate (32%, w/w), sodium starch glycolate (3%, w/w), and magnesium stearate (1%, w/w). This formulation is typical of many immediate release pharmaceutical tablets, and it was produced by blending the excipients in a twin-shell mixer. The compacts were compressed from the blend using a single-station eccentric tablet press (F-press, Manesty, Knowsley, UK) fitted with 8 mm flat face tooling, at a rate of 60 tablets per minute. The powder fill level was adjusted to give tablets with a mean mass of 263 mg, and the minimum punch separation was varied to produce tablets over a range of solid fractions. In the current study, tablets with a solid fraction of 0.90 (at the apparent density of 1380 kg/m^3) were selected for characterization using the acoustic and X-ray tomography methods. A photograph of the five compacts prepared for the pitch-catch attenuation experimental setup (described above) can be found in Fig. 2 (as an inset) and dimensions and material properties are reported in Table 1.

5. Contact ultrasonic experiments

In the pitch-catch attenuation experimental setup (Setup A), an electrical pulse is generated by the pulser/receiver unit which excites Transducer 1, causing an acoustic (elastic wave) pulse to be transmitted through the delay line and compact, to be ultimately received by Transducer 2. In the pitch-catch calibration test (Setup B), the acoustic pulse enters the delay line from Transducer 1, passes through the delay line, and is finally received by Transducer 2. There is no compact use in the calibration measurements. In each case the acoustic pulse obtained by Transducer 2 is converted back to an electrical pulse, which is then received by the pulser/receiver unit and acquired and saved as a digital waveform by the digitizing oscilloscope. A computer with signal processing software is used to analyze the waveform. During experiments, the pulser/receiver unit was set to a pulse repetition frequency (PRF) of 200 Hz, a pulser voltage of 100 V, an amplification gain of 0, a central frequency of 2–2.25 MHz, and the high pass filter (HPF) and low pass filter (LPF) were respectively dialed to the "Out" and "Full Bandwidth" settings to allow the entire frequency spectrum of the transducers to pass through the compact.

While Eq. (2) suffices for calculating attenuation through one continuum structure, in the experimental and calibration setups (Setups A and B, respectively) it accounts for no contact

Table 1
Geometric and material properties.

	m (mg)	h (mm)	D (mm)	ρ (kg/m^3)	c_L (m/s)	E (GPa)	Z (MRayl)
Compact D01	266	3.71	8.15	1370	1540	3.26	2.12
Compact D02	262	3.60	8.21	1370	1520	3.16	2.08
Compact D03	263	3.63	8.14	1390	1560	3.41	2.18
Compact D04	262	3.63	8.12	1390	1530	3.26	2.11
Compact D05	262	3.62	8.17	1380	1550	3.30	2.14
Rexolite® Delay	934	4.08	16.7	1050	2280	5.44	2.39
Transducer 1							7.63
Transducer 2							8.76

interfaces. As shown in Fig. 1b and d, at each of the interfaces there is a transmission coefficient that accounts for the fraction of the total amplitude that is transmitted to the next medium, and, correspondingly, the fraction of total signal amplitude that is reflected back toward the wave source. Since Setups A and B include transmission coefficients, the attenuation expression in Eq. (2) must include the effects of these coefficients. From Fig. 1b and d, an expression for the attenuation in Np/m, including transmission coefficients, can be determined. Setups A and B differ only in that Setup A features the compact. Therefore, by comparing the wave responses captured by each respective configuration, the extent of ultrasonic attenuation in the compact can be found. The first response captured by Transducer 2 in Setup A (Fig. 1b) is $A_f^{T2}(t)$. Likewise, the first response obtained by Transducer 2 in Setup B (Fig. 1d) is $B_f^{T2}(t)$. Based on the path tracing diagrams in Fig. 1b and d, the amplitudes of these pulses can be represented as follows:

$$A_f^{T2}(t) = A_i^{T1} c_T^{T1,R} e^{-\alpha_R h_R} c_T^{R,C} e^{-\alpha_C h_C} c_T^{C,T2} \tag{8}$$

$$B_f^{T2}(t) = B_i^{T1} c_T^{T1,R} e^{-\alpha_R h_R} c_T^{R,T2} \tag{9}$$

where A_i^{T1} is the initial longitudinal wave pulse generated within Transducer 1 in Setup A, $c_T^{T1,R}$ the transmission coefficient at the Transducer 1-delay line interface, α_R the attenuation coefficient of the delay line material, h_R the height of the delay line, $c_T^{R,C}$ the transmission coefficient at the delay line–compact interface, α_C the attenuation coefficient in the compact, h_C the height of the compact, $c_T^{C,T2}$ the transmission coefficient at the compact–Transducer 2 interface, B_i^{T1} the initial longitudinal wave pulse excited within Transducer 1 in Setup B (identical to A_i^{T1}), and $c_T^{R,T2}$ the transmission coefficient at the delay line–Transducer 2 interface.

By dividing Eq. (8) by Eq. (9) and cancelling like terms, the following relation for the ratio of A_f^{T1} to B_f^{T1} is found:

$$\frac{A_f^{T2}(t)}{B_f^{T2}(t)} = \frac{A_i^{T1} c_T^{T1,R} e^{-\alpha_R h_R} c_T^{R,C} e^{-\alpha_C h_C} c_T^{C,T2}}{B_i^{T1} c_T^{T1,R} e^{-\alpha_R h_R} c_T^{R,T2}} = \frac{c_T^{R,C} e^{-\alpha_C h_C} c_T^{C,T2}}{c_T^{R,T2}} \tag{10}$$

Solving Eq. (10) for the attenuation coefficient α_C in the compact material yields:

$$\alpha_C(f) = \frac{1}{h_C} \ln\left(\frac{B_f^{T2}(f)}{A_f^{T2}(f)} \frac{c_T^{R,C} c_T^{C,T2}}{c_T^{R,T2}} \right) \tag{11}$$

where $A_f^{T2}(f)$ and $B_f^{T2}(f)$ have been converted to frequency dependent functions for the purpose of calculating the attenuation coefficient, a frequency dependent coefficient. Since the transmission coefficients $c_T^{R,C}$, $c_T^{C,T2}$, and $c_T^{R,T2}$ are unknown prior to the experiment, two pulse-echo experiments were implemented to determine these remaining coefficients. In order to obtain the transmission coefficients, the acoustic impedances of the compact, delay line, and Transducer 2 material are determined experimentally. As geometric and material properties for the compacts and the delay line are known (Table 1), the acoustic impedance, Z, in Rayl, of these materials is given by:

$$Z = \rho c_L \tag{12}$$

where ρ is the bulk density (kg/m^3), and c_L the longitudinal velocity of sound in the medium (m/s). From the acoustic impedances, the reflection coefficient at the interface between two materials, $C_R^{1,2}$, is given by:

$$C_R^{1,2} = \frac{Z_2 - Z_1}{Z_2 + Z_1} \tag{13}$$

where Z_1 is the acoustic impedance of material 1, and Z_2 the acoustic impedance of material 2. From the reflection coefficient, $C_R^{1,2}$, the corresponding transmission coefficient, $C_T^{1,2}$, is determined by:

$$C_T^{1,2} = 1 - C_R^{1,2} \tag{14}$$

To calculate the acoustic impedance of the Transducer 2 material, two pulse-echo experiments were conducted to determine the reflection coefficient between the delay line, with known acoustic impedance, and the Transducer 2 material. From this reflection coefficient, the acoustic impedance of the transducer material is found using:

$$Z_2 = Z_1 \frac{1 + C_R^{1,2}}{1 - C_R^{1,2}} \tag{15}$$

Calculated values for Z_{Compact}, Z_{Rexolite}, and $Z_{\text{Transducer2}}$ are summarized in Table 1, along with other geometric and material properties. The calculated values for the transmission coefficients are as follows: $c_T^{R,C} = 0.940$, $c_T^{C,T2} = 0.389$, and $c_T^{R,T2} = 0.428$.

6. Data analysis

To determine the attenuation coefficient, the waveforms acquired in Setups A and B, corresponding to A_f^{T2} and B_f^{T1}, were compared in the spectral domain. To facilitate this analysis, the waveforms acquired from Setups A and B, $A_f^{T2}(t)$ and $B_f^{T2}(t)$, sampled by the digitizing oscilloscope (Fig. 3a and b), were Fourier-transformed into the frequency domain waveforms $A_f^{T2}(f)$ and $B_f^{T2}(f)$ using a Fast Fourier Transform (FFT) routine. $A_f^{T2}(f)$ and $B_f^{T2}(f)$ are plotted simultaneously, for amplitude comparison, in Fig. 4. From $A_f^{T2}(f)$ and $B_f^{T2}(f)$ the attenuation coefficient was calculated, based on Eq. (11), by comparing the two waveforms at corresponding frequency values over the operational frequency range (i.e., 0–4 MHz) of Transducers 1 and 2. To determine the directional dependence of the attenuation coefficient, the compacts were examined using two different experimental configurations that varied the vertical orientation of the tablet during testing. As a result of this examination, the ultrasonic attenuation was found to be independent of the propagation direction over the operational frequency range of the transducers.

The attenuation profiles found according to Eq. (11) and presented in Fig. 5 were then analyzed, within the frequency

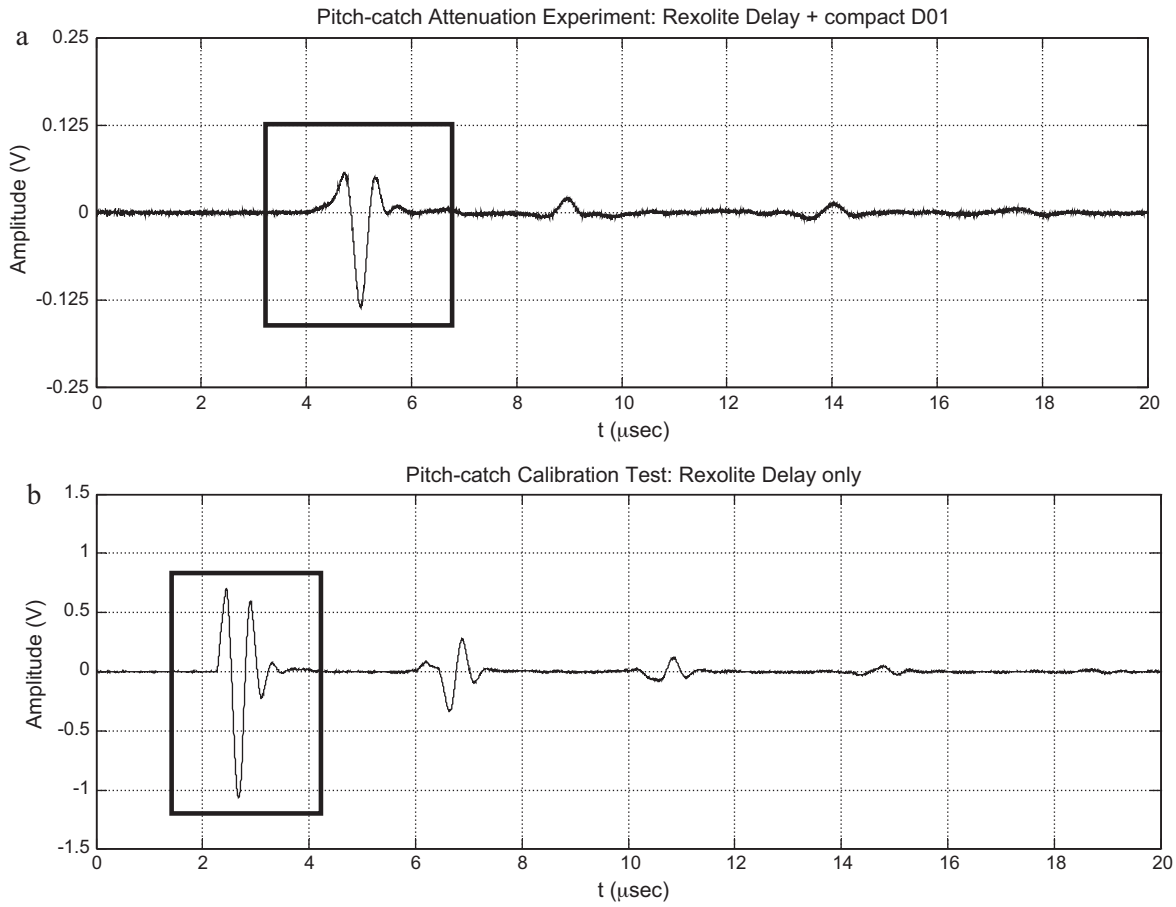

Fig. 3. (a) The first pulse (marked by a square) received by Transducer 2 in the pitch-catch experimental setup (Setup A) – $A_f^{T2}(t)$. (b) The first pulse (marked by a square) received by Transducer 2 in the pitch-catch calibration test setup (Setup B) – $B_f^{T2}(t)$.

bandwidth of the transducers, using the exploratory data analysis procedure proposed by Botvina et al. (2000). As the grain sizes in the tested pharmaceutical compacts are all significantly smaller than the acoustic wavelengths used during experimentation (i.e., $\lambda \gg D$), the grain scattering attenuation is expected to demonstrate strong adherence to the Rayleigh scattering theory (Eq. (5)). However, analysis of Fig. 5 reveals that the attenuation coefficient significantly deviates from the fourth power frequency dependence that is characteristic of Rayleigh scattering. The presence of a non-fourth order dependence on frequency suggests that the primary scattering mechanism in the tested pharmaceutical powder compacts is other than Rayleigh's. This observed deviation from the Rayleigh scattering theory has also been reported by previous authors. Specifically, Botvina et al. (2000) studied polycrystalline microstructures where $D/\lambda < 1$, for which the presence of Rayleigh scattering and the attenuation data's adherence to the fourth power frequency dependence is expected. However, their published results indicate a dominant presence of non-Rayleigh

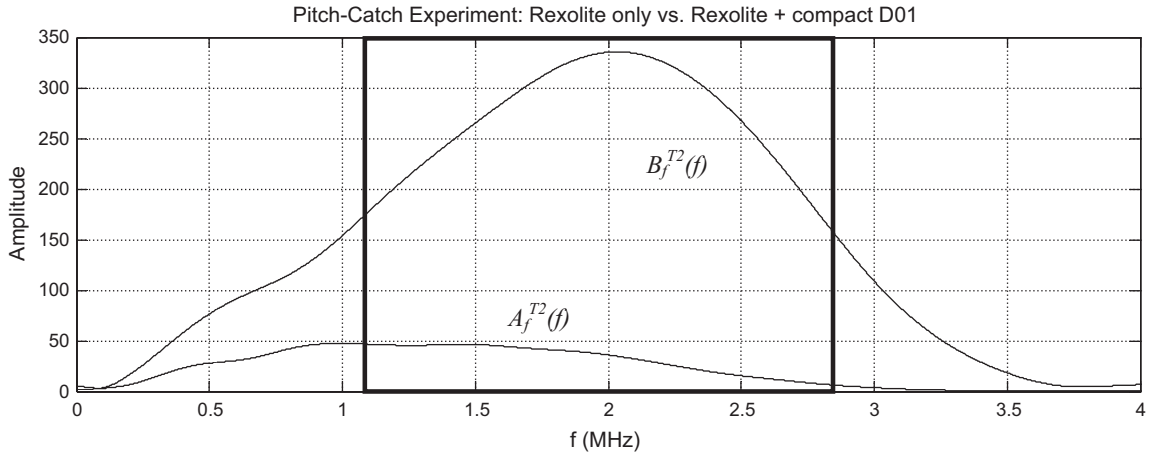

Fig. 4. The amplitudes of the first pulses received by Transducer 2 in Setups A and B, $A_f^{T2}(f)$ and $B_f^{T2}(f)$, plotted in the spectral domain. The transducer frequency bandwidth (1.10–2.80 MHz) is emphasized with a box.

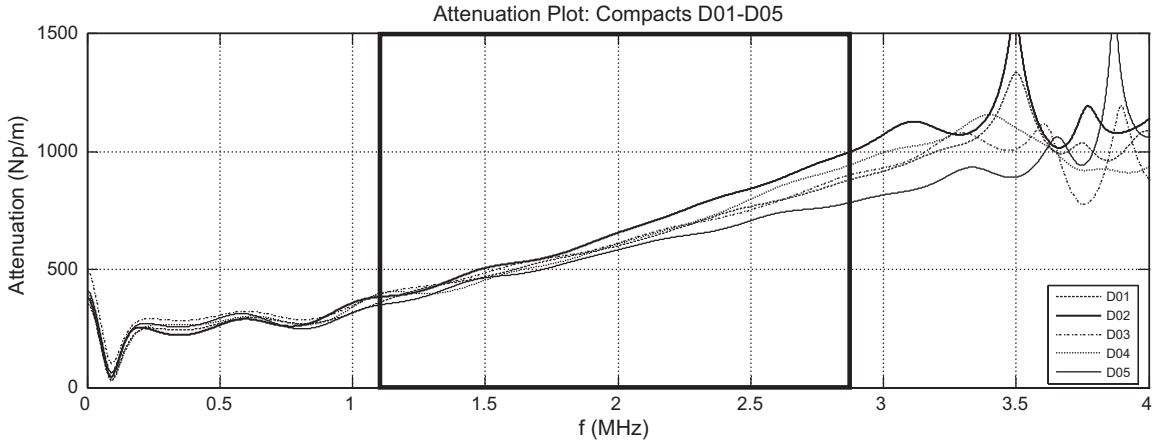

Fig. 5. Frequency dependent attenuation plot for compacts D01–D05. The transducer frequency bandwidth is emphasized with a box.

scattering mechanisms and the implied emergence of multiple scattering. It is noteworthy that previous studies (Nicoletti and Anderson, 1997; Papadakis, 1965) have suggested the necessity of incorporating grain size distributions into the measurement of the frequency dependent attenuation coefficient. Exploratory data analysis of the attenuation profiles in Fig. 5 insinuates that the fourth power frequency dependence may be restored when a distribution of grains is considered. These results, however, are not conclusive.

As their attenuation data deviates significantly from the behavior predicted by the classical scattering regimes, Botvina et al. (2000) employed an exploratory data analysis routine to develop an alternative expression for the relationship between ultrasonic attenuation and grain size (a piecewise linear function) to describe the attenuation behavior in polycrystalline materials, for which the predictions of the classical scattering regimes are inadequate. As this inadequacy has also been observed for the attenuation profiles presented in the current study, the piecewise function was subsequently applied to the plots in Fig. 5 for the determination of the mean grain diameter in the tested pharmaceutical powder compacts. The piecewise linear function is a relation between the dimensionless variables $\log(c_L \times d\alpha/df)$ and $\log(D\alpha)$. The linear portion of the piecewise function corresponding to high attenuating materials, such as pharmaceutical powder compacts (where $\log(c_L \times d\alpha/df) > -1.5$) is as follows:

$$\log(D\,\alpha(f)) = 2\,\log\left(c_L \frac{d\alpha}{df}\right) - 1 \tag{16}$$

where D is the mean grain size or microstructure characteristic length scale (m), α the attenuation coefficient (Np/m), c_L the longitudinal velocity of sound in the compact material (m/s), and f the frequency (Hz). Solving Eq. (16) for D yields:

$$D(f) = \frac{1}{10}\frac{1}{\alpha(f)}\left(c_L \frac{d\alpha}{df}\right)^2 \tag{17}$$

The mean grain diameter sizes for the powder compacts in the current study were established by finding the overall slope and average attenuation coefficient of the attenuation profiles in Fig. 5, for the frequency domain within the bandwidth of the transducers (i.e., 1.10–2.80 MHz). While the overall slope and average attenuation coefficient are used in the establishment of the mean grain diameter of the tested material, the local deviations in the slope of the attenuation curve from the overall trend can be analyzed to ascertain a characteristic length scale profile, revealing the presence of a size distribution within the compact microstructure (Fig. 6). Despite the existence of a distribution of characteristic length scale sizes, the length scale plots generated from this analysis are able to effectively reveal the mean grain diameter, as presented in Fig. 7. Instead of exclusively considering the average slope and average attenuation coefficient over the transducer bandwidth, this graphical analysis involves the calculation of the instantaneous slope and attenuation coefficient at each point within the operational frequency range of the transducers (i.e., 0–4 MHz), and then the identification of the constant region, existing within the transducer bandwidth, from which the mean grain diameter can be extracted.

7. Discussions

Botvina et al. (2000) argued that the piecewise linear function in Eq. (16) be used to establish the mean grain diameter of a polycrystalline microstructure, using attenuation coefficient data over a range of frequencies. This approach was implemented for pharmaceutical powder compacts by applying Eq. (17) to the frequency dependent attenuation profiles in Fig. 5. As described above, there are two methods of extracting the mean grain diameter from the frequency dependent attenuation data. The first method involves the calculation of the overall slope and attenuation coefficient for each attenuation profile, over the frequency bandwidth range of 1.10–2.80 MHz. The mean grain diameters calculated using this method are as follows: D01: 35.3 μm, D02: 42.1 μm, D03: 34.0 μm, D04: 37.8 μm, and D05: 25.4 μm. The second method involves plotting all the detected length scale sizes using Eq. (17), and identifying the region within the transducer bandwidth for which the length scale sizes are generally constant and oscillate around a central mean grain diameter. From analysis of Fig. 6, the region within the transducer bandwidth that demonstrates the most consistent length scale behavior, indicating the predominant mean grain diameter, is between 1.50 and 2.80 MHz (this region is emphasized on Fig. 6). Though the transducer bandwidth extends from 1.10 to 2.80 MHz, the lower end of the bandwidth range (1.10–1.50 MHz) does not demonstrate a consistent oscillatory pattern but in places shows great variability (refer to Fig. 6). The consistent oscillatory pattern revealing the predominant mean grain diameter does not completely begin until about 1.50 MHz and extends to 2.80 MHz. For this reason, the frequency range used for the graphical analysis procedure described above was chosen as 1.50–2.80 MHz.

Under ideal conditions, namely a narrow length scale distribution within the compact, adherence to a single scattering regime, and the overall validity of the single scattering assumption, the mean grain diameter within this frequency domain should appear as a straight line, instead of exhibiting oscillatory behavior as seen in Fig. 6. However, the observed oscillatory behavior indicates a deviation from ideality in the compact internal microstructure.

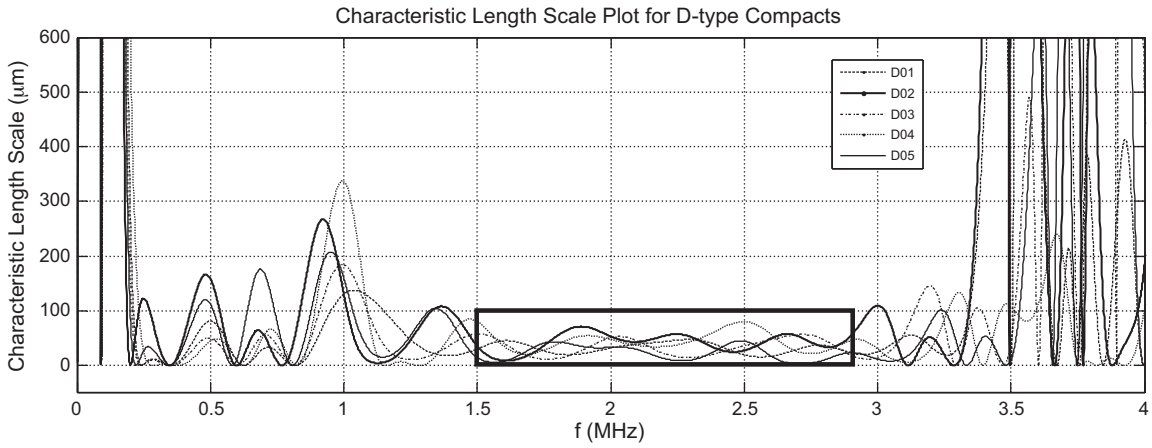

Fig. 6. Characteristic length scale profiles for compacts D01–D05-based on the frequency dependent attenuation plots presented in Fig. 5. The mean grain diameters are calculated graphically over the frequency range of 1.50–2.80 MHz (emphasized with a box).

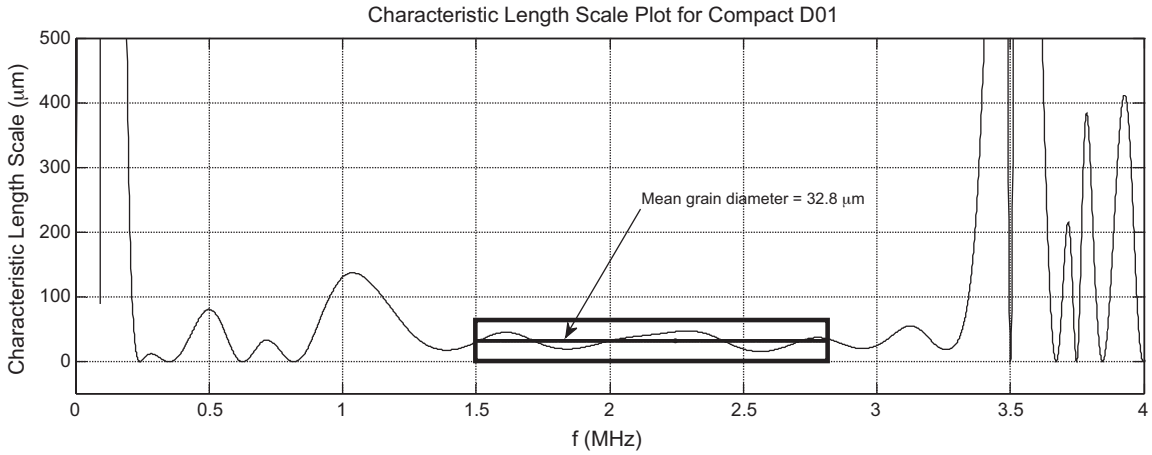

Fig. 7. Characteristic length scale profile for compact D01. The mean grain diameter, for the frequency range of 1.50–2.80 MHz, is shown on the plot. The mean grain diameters, respectively, are obtained as 32.8, 42.3, 34.7, 45.3, and 23.4 μm for D01–D05.

The presence of a discernable length scale distribution, as well as the conglomeration of particles, during compaction, into larger microstructural features, suggests that the grain scattering occurring within the transducer bandwidth may be a result of the coalescence of more than one scattering mechanism. Analogously, past authors have also concluded that their results implied the presence of multiple scattering effects, and thus an unexpected transition from the classical Rayleigh regime to a regime resembling that of the stochastic. In fact, Botvina et al. (2000) reported the presence of more than one scattering mechanism in the surveyed data, and postulated that the presence of grain distributions could cause the scattering attenuation to exhibit behavior independent of simply one classical scattering regime. Given the similarity between past authors' conclusions and the deviation from ideality apparent within the materials tested in the current study, it is highly likely that the oscillatory behavior seen in Fig. 6 is a result of the presence of multiple scattering, characteristic length scale distributions, and the effects of several scattering mechanisms operating simultaneously. Despite non-ideal conditions, the extraction of mean grain diameters from Fig. 6 is warranted, as it is evident that the characteristic length scale plots do not oscillate haphazardly within the frequency range 1.50–2.80 MHz, but instead do so about a discernable mean grain diameter size.

In order to extract the mean grain diameter from each length scale profile, the average value of each curve in Fig. 6, in the frequency domain 1.50–2.80 MHz, was calculated. These values were then plotted as horizontal lines over the frequency range of interest to reveal the mean grain diameter around which each characteristic length scale plot oscillates. This graphical method is shown for compact D01 in Fig. 7. The mean grain diameters calculated using this method are as follows: D01: 32.8 μm, D02: 42.3 μm, D03: 34.7 μm, D04: 45.3 μm, and D05: 23.4 μm. Comparison between the mean grain diameters derived from both methods of analysis reveals that the two methods are consistent (Table 2).

In order to confirm the accuracy of the mean grain diameters calculated using Eq. (17), an independent MicroXCT image (XCT200, X-Radia Inc., California) of a similar pharmaceutical compact was analyzed by straight line tomography for the purpose of extracting a verifiable mean grain diameter (Figs. 8 and 9). The mean grain size

Table 2
Mean characteristic length scale size predictions.

Compacts	Length scale sizes (μm)		
	Ultrasonic methods		MicroXCT
	1	2	
D01	35.3	32.8	39.0
D02	42.1	42.3	
D03	34.0	34.7	
D04	37.8	45.3	
D05	25.4	23.4	
Average	34.9	35.7	39.0

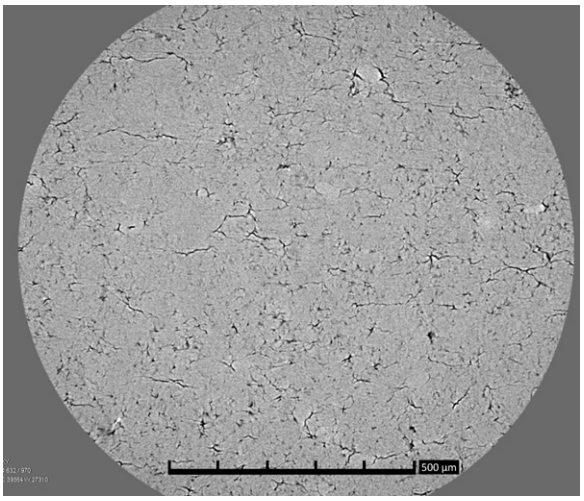

Fig. 8. MicroXCT image of pharmaceutical compact – the distribution of characteristic length scales and individual grain sizes is visible. The field of view in the image represents only a localized portion of the analyzed compact. A 500 μm scale bar has been included to illustrate the size of the various microstructure features.

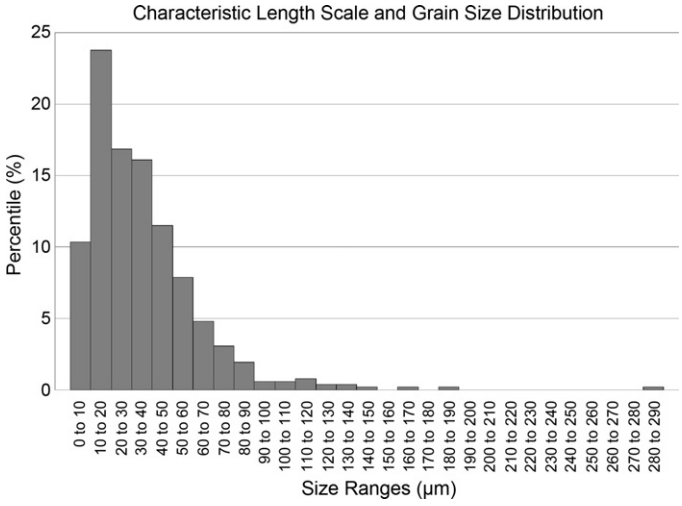

Fig. 9. Characteristic length scale and grain size distribution histogram – based on analysis of the MicroXCT image shown in Fig. 8. The mean grain diameter size is 39.0 μm.

acquired for the MicroXCT image was 39.0 μm. Due to the general agreement between the ultrasonic attenuation derived mean grain diameter and the MicroXCT derived results (Table 2), the proposed approach appears to be an effective method for determining the mean grain diameter sizes for pharmaceutical powder compacts.

While the mean grain diameters predicted from the ultrasonic attenuation technique essentially match that found with MicroXCT, there are minor discrepancies in the results likely caused by the variable size distributions between compacts. It may be that larger sample sizes for the ultrasonic attenuation and MicroXCT techniques would eliminate the deviation from uniformity that appears when the two sets of results are compared. However, despite these discrepancies, the mean grain diameters ascertained from the ultrasonic attenuation technique are consistent with the results of the MicroXCT analysis.

8. Conclusions and remarks

As the microstructure of a pharmaceutical compact has a considerable influence on its mechanical properties and thus therapeutic effectiveness as a drug delivery vehicle, a more efficiently apprehended and comprehensive understanding of a compact's microstructure is highly desired. In the current study, an ultrasonic attenuation technique was applied to experimentally predict the characteristic grain size in pharmaceutical compacts made from pharmaceutical grade MCC–LMH blended excipient powder, at a solid fraction of 0.90. The mean grain diameter was approximated by analyzing the frequency dependent attenuation coefficient generated by comparing the output waveforms from two ultrasonic non-destructive pitch-catch experiments. The results derived from this method were then compared to the mean grain size obtained by straight line tomography measurements of an independently acquired MicroXCT scan. The ultrasonic attenuation technique, upon comparison with the MicroXCT-derived results, was revealed as an effective procedure for non-destructively and rapidly establishing the mean grain diameter in MCC–LMH pharmaceutical compacts. The ultrasonic attenuation and MicroXCT methods predicted mean grain diameters of approximately 35.3 μm and 39.0 μm, respectively (Table 2).

While the ultrasonic attenuation technique shows promise of becoming an effective method to experimentally determine the mean grain diameter size within pharmaceutical compacts, further testing with alternative materials featuring solid fractions other than 0.90 is necessary to confirm this method's applicability to other solid fraction ranges and the diverse microstructural forms that appear throughout the pharmaceutical industry. In the future, the degree of statistical and experimental rigor around the comparison of the ultrasonic attenuation and MicroXCT techniques could potentially be increased as well. Namely, the acquisition of a larger set of MicroXCT images, processed by more powerful image processing software, along with additional compact samples, would serve to more fully populate the data presented in this research and in so doing provide a greater degree of statistical certainty when comparing the results of the ultrasonic attenuation and MicroXCT techniques.

Acknowledgements

Partial funding and compacts utilized in this study were provided by Pfizer Inc. Special thanks are due to Jack Coats of X-Radia, Inc., for providing MicroXCT images of compact samples, and the Pharmaceutical Development Group at Pfizer Global Research & Development in Groton, CT, for providing the first author (CJS) the opportunity to participate in a unique and stimulating research project as a part of Pfizer's Summer Student Work Program.

References

Abdullah, B., Lajci, A., Shehu, V., Krasniqi, S., Islami, H., 2010. Study of formulation of pharmaceutical forms of paracetamol in medical practice. Med. Arh. 64, 196–199.

Adolfsson, Å., Olsson, H., Nyström, C., 1997. Effect of particle size and compaction load on interparticulate bonding structure for some pharmaceutical materials studied by compaction and strength characterisation in butanol. Eur. J. Pharm. Biopharm. 44, 243–251.

Akseli, I., Becker, D.C., Cetinkaya, C., 2009a. Ultrasonic determination of Young's moduli of the coat and core materials of a drug tablet. Int. J. Pharm. 370, 17–25.

Akseli, I., Hancock, B.C., Cetinkaya, C., 2009b. Nondestructive determination of anisotropic mechanical properties of pharmaceutical dosage forms. Int. J. Pharm. 377, 35–44.

Akseli, I., Cetinkaya, C., 2008a. Acoustic testing and characterization techniques for pharmaceutical solid dosage forms. J. Pharm. Innov. 3, 4216–4226.

Akseli, I., Cetinkaya, C., 2008b. Drug tablet thickness estimations using air-coupled acoustic. Int. J. Pharm. 351, 165–173.

Akseli, I., Cetinkaya, C., 2008c. Air-coupled non-contact mechanic property determination of drug tablets. Int. J. Pharm. 359, 25–34.

Akseli, I., Dipankar, D., Cetinkaya, C., 2010. Mechanical property characterization of bilayered tablets using non-destructive air-coupled acoustics. AAPS PharmSciTech 11, 90–102.

Akseli, I., Libordi, C., Cetinkaya, C., 2008a. Real-time acoustic elastic property monitoring of compacts during compaction. J. Pharm. Innov. 3, 134–140.

Akseli, I., Mani, G.N., Cetinkaya, C., 2008b. Non-destructive acoustic defect detection in drug tablets. Int. J. Pharm. 360, 65–76.
Alderborn, G., Nystrom, C., 1982. Studies on direct compression of tablets: Part 4. Effect of particle size on the mechanical strength of tablets. Acta Pharm. Suec. 19, 381–390.
Azarmi, S., Roa, W., Lobenberg, R., 2007. Current perspectives in dissolution testing of conventional and novel dosage forms. Int. J. Pharm. 328, 12–21.
Botvina, L.R., Fradkin, L.J., Bridge, B., 2000. A new method for assessing the mean grain size of polycrystalline materials using ultrasonic NDE. J. Mater. Sci. 35, 4673–4683.
Djemai, A., Sinka, I.C., 2006. NMR imaging of density distributions in tablets. Int. J. Pharm. 319, 55–62.
Dokoumetzidis, A., Macheras, P., 2006. A century of dissolution research: from Noyes–Whitney to the biopharmaceutics classification system. Int. J. Pharm. 321, 1–11.
Eiliazadeh, B., Briscoe, B.J., Sheng, Y., Pitt, K., 2003. Investigating density distributions for tablets of different geometry during the compaction of pharmaceuticals. Particul. Sci. Technol. 21, 303–316.
Fu, X., Dutt, M., Bentham, A.C., Hancock, B.C., Cameron, R.E., Elliott, J.A., 2006a. Investigation of particle packing in model pharmaceutical powders using X-ray microtomography and discrete element method. Powder Technol. 167, 134–140.
Fu, X., Elliott, J.A., Bentham, A.C., Hancock, B.C., Cameron, R.E., 2006b. Application of X-ray microtomography and image processing to the investigation of a compacted granular system. Part. Part. Syst. Charact. 23, 229–236.
Gane, P.A.C., Ridgway, C.J., Barcelo, E., 2006. Analysis of pore structure enables improved tablet delivery systems. Powder Technol. 169, 77–83.
Hiestand, E.N., 2003. Mechanics and Physical Principles for Powders and Compacts. SSCI Inc, West Lafayette, IN, USA.
Lewis, C.J., Train, D., 1965. An investigation of die wall friction during the compaction of powders. J. Pharm. Pharmacol. 17, 1–9.
Narayan, P., Hancock, B.C., 2003. The relationship between the particle properties, mechanical behavior, and surface roughness of some pharmaceutical excipient compacts. Mater. Sci. Eng. A 355, 24–36.
Narayan, P., Hancock, B.C., 2005. The influence of particle size on the surface roughness of pharmaceutical excipient compacts. Mater. Sci. Eng. A. 407, 226–233.
Hussain, A.S., Watts, C., Afnan, A.M., Wu, H., 2004. Foreword. J. Process Anal. Technol. 1, 3–4.
Jounela, A.J., Pentikainen, P.J., Sothmann, A., 1975. Effect of particle size on the bioavailability of digoxin. Eur. J. Clin. Pharmacol. 8, 365–370.
Lee, J., 2003. Drug nano- and microparticles processed into solid dosage forms: physical properties. J. Pharm. Sci. 92, 2057–2068.
Levy, G., 1963. Effect of particle size on dissolution and gastrointestinal absorption rates of pharmaceuticals. Am. J. Pharm. Sci. Support. Public Health 135, 78–92.
Morse, P.M., 1936. Vibration and Sound. McGraw-Hill, New York, pp. 257, 269.
Nicoletti, D., Anderson, A., 1997. Determination of grain-size distribution from ultrasonic attenuation: transformation and inversion. J. Acoust. Soc. Am. 101, 686–689.
Nowacki, K., 2009. Possibility of determining steel grain size using ultrasonic waves. Metalurgija 48, 113–115.
Oberholzer-Gee, F., Inamdar, S.N., 2004. Merck's recall of Rofecoxib – a strategic perspective. N. Engl. J. Med. 351, 2147–2149.
Papadakis, E.P., 1965. Revised grain scattering formulas and tables. J. Acoust. Soc. Am. 37, 703–717.
Podczeck, F., 1998. Measurement of surface roughness of tablets made from polyethylene glycol powders of various molecular weight. Pharm. Pharmacol. Commun. 4, 179–182.
Roggo, Y., Chalus, P., Maurer, L., Lema-Martinez, C., Edmond, A., Jent, N., 2007. A review of near infrared spectroscopy and chemometrics in pharmaceutical technologies. J. Pharm. Biomed. Anal. 44, 683–700.
Roney, R.K., 1950. The influence of metal grain size on the attenuation of an ultrasonic wave. Ph.D Thesis. California Institute of Technology.
Saravanan, M., Nataraj, K.S., Ganesh, K.S., 2002. The effect of tablet formulation and hardness on in vitro release of cephalexin from eudragit l100 based extended release tablets. Biol. Pharm. Bull. 25, 541–545.
Sarpun, I.H., Kilickaya, M.S., 2006. Mean grain size determination in marbles by ultrasonic first backwall echo height measurements. NDT E Int. 39, 82–86.
Sinka, I.C., Burch, S.F., Tweed, J.H., Cunningham, J.C., 2004. Measurement of density variations in tablets using X-ray computed tomography. Int. J. Pharm. 271, 215–224.
Sun, C.Q., Grant, D.J.W., 2001. Effects of initial particle size on the tableting properties of L-lysine monohydrochloride dihydrate powder. Int. J. Pharm. 215, 221–228.
Varghese, I., Cetinkaya, C., 2007. Non-contact photo-acoustic defect detection in drug tablets. J. Pharm. Sci. 96, 2125–2133.